Chin. Phys. Lett. **39**, 057301 (2022)

Lieb Lattices Formed by Real Atoms on Ag(111) and Their Lattice Constant-Dependent Electronic Properties

Xiaoxia Li(李小霞)[1†], Qili Li(李启立)[1†], Tongzhou Ji(吉同舟)[1], Ruige Yan(闫睿戈)[1], Wenlin Fan(范文琳)[1], Bingfeng Miao(缪冰锋)[1,2], Liang Sun(孙亮)[1,2], Gong Chen(陈宫)[1,2], Weiyi Zhang(章维益)[1,2], and Haifeng Ding(丁海峰)[1,2*]

[1]*National Laboratory of Solid State Microstructures and Department of Physics, Nanjing University, Nanjing 210093, China*
[2]*Collaborative Innovation Center of Advanced Microstructures, Nanjing 210093, China*

(Received 10 February 2022; accepted 28 March 2022; published online 26 April 2022)

Scanning tunneling microscopy is a powerful tool to build artificial atomic structures that do not exist in nature but possess exotic properties. In this study, we constructed Lieb lattices with different lattice constants by real atoms, i.e., Fe atoms on Ag(111), and probed their electronic properties. We obtain a surprising long-range effective electron wavefunction overlap between Fe adatoms as it exhibits a $\frac{1}{r^2}$ dependence with the interatomic distance r instead of the theoretically predicted exponential one. Combining control experiments, tight-binding modeling, and Green's function calculations, we attribute the observed long-range overlap to being enabled by the surface state. Our findings enrich the understanding of the electron wavefunction overlap and provide a convenient platform to design and explore artificial structures and future devices with real atoms.

DOI: 10.1088/0256-307X/39/5/057301

Artificial atomic structures built by scanning tunneling microscopy (STM) are a fertile playground to investigate fundamentals and explore potential applications. For instance, logic gates are realized by CO molecule cascades on Cu(111)[1] and Fe elliptical quantum corrals on Ag(111).[2] Quantum holographic encoding of CO on Cu(111) achieves information densities in excess of 20 bits/nm^2.[3] A kilobyte rewritable atomic memory is presented for Cl vacancies on Cu(100).[4] Fundamentally, Au atomic chains on NiAl(110) demonstrate the development of a one-dimensional band structure.[5] Spin–spin interactions are probed for Mn chains on CuN on Cu(100).[6] Majorana bound states are observed at the ends of chains for Fe on Pb(110)[7–9] and Re(0001).[10] Two-dimensional structures have been widely studied for quantum size effect in nanocorrals,[11–13] Dirac fermions in molecular graphene of CO on Cu(111),[14] quasi-crystals in Penrose tiling of CO on Cu(111),[15] and fractals in Sierpiński triangle CO on Cu(111).[16]

Lieb lattice,[17] a two-dimensional square lattice consisting of an atom at the corner and two atoms at the middle of each edge, has attracted significant attention because of its exotic electronic band structure and predicted unusual properties in ferromagnetism,[17–20] superconductivity[21–23] and topological states,[24–26] even though it does not exist in nature. Recently, Lieb lattices have been experimentally realized in optical[27–30] and electronic systems with artificial objects.[31–34] As previously mentioned, STM naturally has the advantage of studying this structure. Lieb lattices have been successfully assembled and investigated with Cl vacancies on Cu(100)[32] and artificial atoms formed by the quantum confinement of the surface state through the CO molecules on Cu(111).[31] It is worth noting that artificial objects are used to mimic the real atoms in the study of Lieb lattices realized by the Cl vacancies and quantum states confined by CO molecules. Therefore, it is essential to construct Lieb lattices with real atoms and investigate their properties.

In the present study, we employ atomic manipulation[35] to construct Lieb lattices with real atoms, i.e., Fe adatoms on Ag(111), instead of the anti-Lieb lattices formed by Cl or CO molecules. We obtain typical features of Lieb lattice by measuring the spectroscopy and differential conductance map. Furthermore, we systematically performed lattice constant-dependent studies by tuning the interatomic distance r through atomic manipulation. Note that the high internal pressure in solid makes it nearly impossible to vary r with large amplitude, which is imperative for the r-dependence studies. Compared with tight-binding modeling, we obtain that the effective overlap energy t shows a $\frac{1}{r^2}$ dependence, in sharp contrast with the theoretically predicted exponential one for the direct overlap between two s states.[36] Combining control experiments and Green's function-

†These authors contributed equally to this work.
*Corresponding author. Email: hfding@nju.edu.cn

based calculations,[37,38] we find that the observed long-range features of Lieb lattices are an indirect interaction between Fe atoms mediated by the surface state.

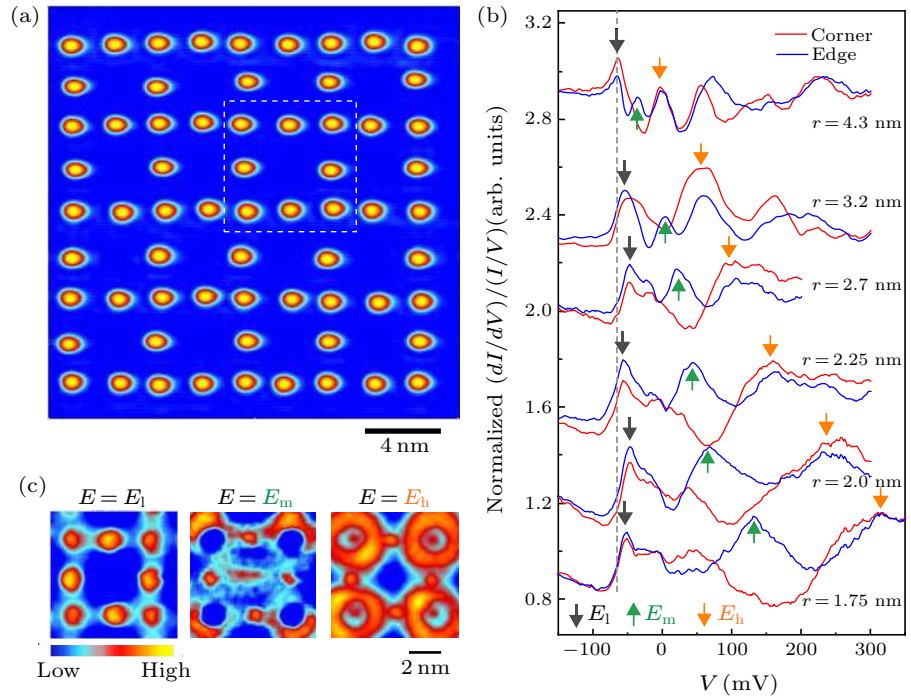

Fig. 1. (a) Typical topographic image of a 4×4 Lieb lattice ($r = 2.25$ nm) constructed with Fe adatoms on Ag(111). (b) Normalized $(dI/dV)/(I/V)$ spectra at corner sites (red) and edge sites (blue) with different r (curves are shifted for clarity). The dashed line indicates the surface state onset energy of Ag(111). Orange, green, and gray arrows represent the high-, middle-, and low-energy peaks, respectively. (c) Typical dI/dV maps obtained at the square area marked in (a) at the low, middle, and high energy peaks.

The experiments were performed in a low-temperature STM system with the base pressure of 2×10^{-11} mbar. The Ag(111) single crystals were prepared with cycles of Ar^+ sputtering (1.5 kV) and annealing (∼580 ℃). High-purity Fe was deposited on the Ag(111) surfaces with a typical rate of 0.002 monolayer equivalent per minute through electron beam evaporation at ∼6 K. The measurements and atomic manipulations are performed with the W tips at ∼4.7 K. We constructed a series of Lieb lattices by laterally manipulating Fe atoms on the Ag(111) surface.[2,35] Figure 1(a) shows a typical topographic image of an assembled 4×4 Lieb lattice ($r = 2.25$ nm). To investigate its electronic properties, we acquire the tunneling current I and the differential conductance (dI/dV) as functions of the bias voltage V on top of the Fe adatoms at the corner and edge sites [Fig. S5(a) in the Supplementary Information] and on an isolated single adatom using the lock-in technique with a modulation of the sample voltage of 4 mV at a frequency of 6.3 kHz [Fig. S4(b)]. The tip stabilizes at 50 mV and 1 nA before the dI/dV measurements. To exclude the tip effect, we normalized the raw data by dividing the $(dI/dV)/(I/V)$ curves of the Fe adatoms in the lattices by the one obtained on top of the isolated Fe adatom with the same tip. The normalization also minimizes the influence of the tunneling matrices.

As shown in Fig. 1(b), at the edge sites (blue curves), the normalized spectra show three pronounced sets of peaks: low-energy peaks (marked by gray arrows) located close to the surface state onset energy (−65 mV; gray dashed line),[39] middle energy peaks (green arrows), and high energy peaks (orange arrows). At the corner sites (red curves), they exhibit only two sets of peaks that coincide with the peaks near the onset energy of the surface state and the high energy peaks obtained at the edge sites. When the r value increases from 1.75 to 4.8 nm, both sets of the middle and high energy peaks shift to lower energy, whereas the low-energy peak remains nearly unchanged. The middle energy peak is located approximately at the energy in the middle of the high and low-energy peaks. It is worth noting that there are other peaks at the energies above these three peaks. They may originate from the scattering of the surface state since Fe adatoms also serve as the scattering centers for the surface state, as confirmed through Green's function calculation in the Supplementary Information. Figure 1(c) shows the measured dI/dV maps for $r = 2.25$ nm at three energies. It shows that the electrons are localized at edges sites at the energy of E_m, whereas they distribute at both the corner and edge sites with energies of E_l and E_h, respectively. The features in the middle of the Lieb lattice at E_m

and the ring-shaped features at $E_{\rm h}$ in Fig. 1(c) are the interference patterns caused by the scattering of the surface state, as discussed in the Supplementary Information. Note that the dI/dV maps were obtained with a constant height mode. Because of the chemical difference, the actual height between the tip and the surface might be different for the tip placed on top of Ag and Fe. Here, we mainly focus on the spectra on top of the Fe adatoms.

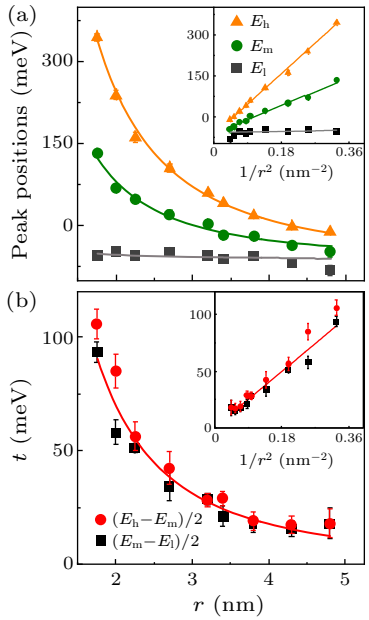

Fig. 2. (a) Peak positions of the normalized differential conductance spectra as a function of r and $1/r^2$ (inset). (b) The comparison of $(E_{\rm h}-E_{\rm m})/2$ and $(E_{\rm m}-E_{\rm l})/2$ as a function of r and $1/r^2$ (inset). The curves outside (inside) the insets are the fittings with the inverse parabolic (linear) function.

To analyze the variation of the peak position with the atomic separation r, we plot $E_{\rm l}$, $E_{\rm m}$, and $E_{\rm h}$ as a function of r in Fig. 2(a). Consequently, we found that both datasets can be fitted with $E = E_0 + \frac{C}{r^2}$, where the value of E_0 is close to the onset energy of the surface state (Table S1). As shown in Fig. 2(b), we also obtained the r-dependent values of $(E_{\rm h}-E_{\rm m})/2$ and $(E_{\rm m}-E_{\rm l})/2$. Interestingly, we obtained that they are very similar within our experimental error margin. As the peak positions $E_{\rm l}$, $E_{\rm m}$, and $E_{\rm h}$ show the $\frac{1}{r^2}$-dependence, we fitted them with $\Delta E = \Delta E_0 + \frac{C_\Delta}{r^2}$. As shown in Fig. 2(b), the fitted curve with fitting parameters $\Delta E_0 = 1.0 \pm 2.2$ meV and $C_\Delta = 273.9 \pm 14.5$ meV·nm^2 reproduces the experimental data well, indicating that half of the peak interval is $\frac{1}{r^2}$-dependent. For clarity, we also plot them as a function of $1/r^2$ and show their linear relationship in the insets of Fig. 2.

To understand the observed electronic properties of the lattices, we first calculated the band structure and the local density of states (LDOS) using the tight-binding method by only considering the s orbitals of the real atoms, implying that no substrate is considered. We set the onsite energy to be zero for the corner and edge sites and the nearest neighboring overlap energy to t. As shown in Fig. 3(a), the band structure features two Dirac bands and a flat band.[40–42] Correspondingly, the LDOS curve shows two peaks at the corner site and three peaks at the edge site, with the middle peak located at the center of the other two peaks. The calculated LDOS maps show that the electrons are mainly localized at edge sites at the middle energy, whereas the electrons are distributed at the corner and edge sites at low and high energies. We only consider the overlap between s orbitals in the above tight-binding calculations. However, the Hamiltonian should also be valid when the nearest neighboring sites have relatively localized states, which overlap with effective overlap energy. For Fe adatom on Ag(111), the 4s state has a strong coupling with the surface state, resulting in relatively localized states. It can be anticipated that the band structure formed by these localized states is similar to the one formed by the s orbitals, except that the onsite and overlap energies are different. Therefore, the tight-binding calculated results essentially reproduce the features on normalized $(dI/dV)/(I/V)$ curves and the dI/dV maps [Figs. 1(b) and 1(c)] observed in our experiments. Thus, the experimentally obtained $E_{\rm l}$, $E_{\rm m}$, and $E_{\rm h}$ are attributed to the characteristic peaks of the Lieb lattice. As shown in Fig. 3(a), the peak interval is $2t$ ($4t$) at the edge (corner) site; i.e., the overlap energy t is $(E_{\rm h}-E_{\rm m})/2$ or $(E_{\rm m}-E_{\rm l})/2$. Thus, the peak intervals in the experimental dI/dV curves correspond to twice the overlap energy, and it is of $\frac{1}{r^2}$ dependence. Note that we only consider the nearest-neighbor hopping in the tight-binding calculation shown in Fig. 3, and the band structure is symmetric around the onsite energy. When the second nearest-neighbor hopping is included, the band structure is no longer symmetric.

However, the observed $\frac{1}{r^2}$-dependent overlap energy in our experiments is in sharp contrast with the exponential dependence predicted in the literature.[36] The prediction was made for the direct overlap between the s states of two hydrogen atoms in free space. The direct overlap energy can be calculated as ~10 meV when their separation is 0.55 nm. In our experiments, the measured overlap energy is about 17 meV, even when r is 4.8 nm. Therefore, the long-range overlap energy we observed on Ag(111) is not the direct overlap between Fe atoms. We attribute the difference between the theoretical prediction and our experiments to the atomic environment as the prediction was made for atoms in free space, while our experiments were conducted with adatoms placed on top of an Ag(111) surface. The latter enables a surface state around the Fermi energy. Moreover, we performed similar measurements on an Ag(100) substrate, which

has no surface state near the Fermi energy. Interestingly, the spectra of the Fe Lieb lattices on Ag(100) do not show any apparent feature of the Lieb lattice (Fig. S10). Instead, the spectra obtained at the corner or edge sites are very similar to the spectrum of the isolated single adatom, even when r approaches only ∼1 nm. The significantly different r-dependences for Fe adatoms on both substrates highlight the crucial role of the surface state on the observed long-range overlap on Ag(111) surface. According to previous studies, the spectrum of the isolated Fe adatom [Fig. S4(b)] shows that the 4s state of Fe strongly overlaps with the surface state, resulting in relatively localized states.[43,44] It can be anticipated that the band structure formed by these localized states is similar to the one formed by the s orbitals, except that the onsite and overlap energies are different. Thus, the electronic features of Lieb lattice are observed at a large atomic separation. This is not too surprising as in the exploration of the quantum mirage, the Kondo resonance peak of Co adatom located at one focus point of elliptical corral can be projected to the other focus point around 10 nm apart on Cu(111) through the surface state.[12] In a similar study, the inversion state of an Fe adatom can also be transferred to another location more than 10 nm apart in Ag(111) through the surface state.[2]

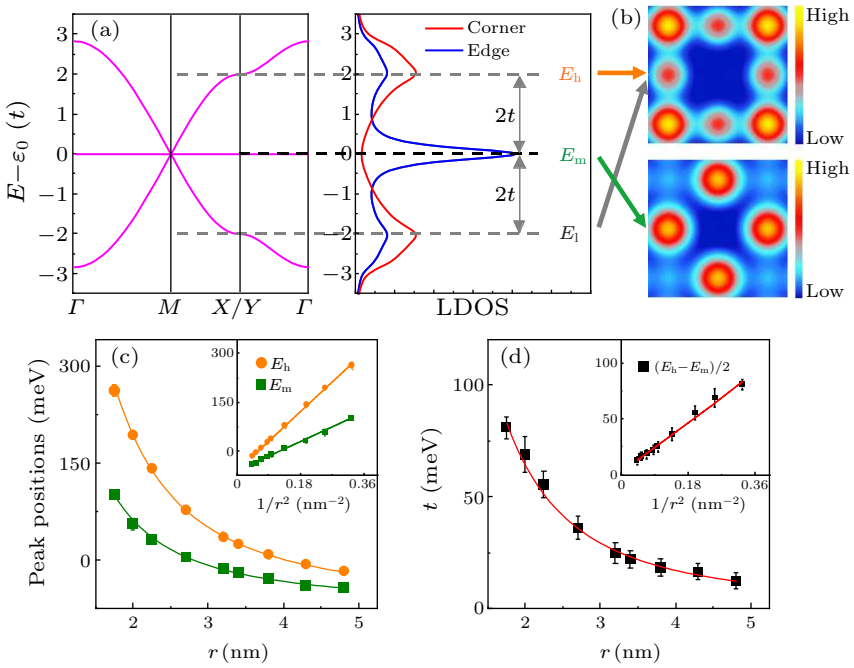

Fig. 3. (a) Calculated band structure of a Lieb lattice and the corresponding LDOS at corner (red) and edge (blue) sites with the effective nearest-neighbor overlap energy t using the tight-binding method. Note: The energy differences among E_h, E_m, and E_l are 2t as marked. (b) LDOS maps at E_h, E_m, and E_l, respectively. (c) Calculated peak positions of a 4×4 Lieb lattice on Ag(111) using Green's function method as a function of r and $1/r^2$ (inset). (d) The corresponding value of $(E_h-E_m)/2$. The curves outside (inside) the insets in (c) and (d) are fittings with the inverse parabolic (linear) functions.

To further verify the essential role of the surface state, we performed Green's function-based calculations for Fe Lieb lattices built on Ag(111). The calculated LDOS curves exhibit close similarity with the experimental dI/dV [Fig. S5(c)]. Note that we mainly consider the surface state in Green's function calculations, which are valid only above the onset of the surface state. The experimentally obtained peak E_l is very close to the onset energy, corresponding to small wavevector and large wavelength. Thus, E_l may be influenced by the onset of the surface state and it is not accurately determined. Therefore, we focus our discussion on E_m and E_h. Figure 3(c) shows the plots of E_m and E_h versus r; they can be fitted well with $E = E_0 + \frac{C}{r^2}$. The value of $(E_h - E_m)/2$ also follows the $\frac{1}{r^2}$ dependence. The fitting parameter $C_\Delta = 249.3 \pm 8.1$ meV·nm^2 is consistent with our experimental result of 273.9 ± 14.5 meV·nm^2. The insets in Figs. 3(c) and 3(d) show the linear dependences of the peak positions and $(E_h - E_m)/2$ versus $1/r^2$, respectively. Note that in Green's function calculation, we consider the scattering of the surface state by the Fe adatom and the coupling of the Fe 4s state and the surface state of Ag(111) with the empirical description of the inversion effect. For more accurate analysis, first-principle calculations may be needed.

In summary, we have successfully constructed the Fe Lieb lattice on Ag(111) surface with real atoms and tuned its electronic properties by varying its atomic separation. It is found that the effective overlap en-

ergy between lattice sites exhibits a $\frac{1}{r^2}$ dependence. Combining the control experiments on Ag(100), tight-binding modeling, and Green's function calculations, we attribute the long-range overlap energy to the effective overlap of Fe adatom mediated by the surface state. It is realized that the hybridization between adatoms and surface state must be sufficiently strong to observe this long-range effect between lattice adatoms. Moreover, it is known that Co, Ag, Cu, and Mn adatoms also show strong hybridization on Ag(111), Cu(111), or Au(111)[37,45–49] besides Fe adatoms. Our experiments provide a convenient platform for designing and exploring artificial structures and devices with various materials combinations and exotic properties, such as flat and topological bands. We note that similar approaches are successfully used to realize atomic systems (with direct bonding),[50,51] flat-band system, molecule graphene, and quasi-crystal (with artificial atoms).[14,15,52]

Acknowledgments. This work was supported by the National Key R&D Program of China (Grant Nos. 2017YFA0303202 and 2018YFA0306004), the National Natural Science Foundation of China (Grant Nos. 11974165, 92165103, 51971110, and 11734006), the China Postdoctoral Science Foundation (Grant No. 2019M651766), and the Natural Science Foundation of Jiangsu Province (Grant No. BK20190057).

References

[1] Heinrich A J, Lutz C P, Gupta J A and Eigler D M 2002 *Science* **298** 1381
[2] Li Q L, Li X X, Miao B F, Sun L, Chen G, Han P and Ding H F 2020 *Nat. Commun.* **11** 1400
[3] Moon C R, Mattos L S, Foster B K, Zeltzer G and Manoharan H C 2009 *Nat. Nanotechnol.* **4** 167
[4] Kalff F E, Rebergen M P, Fahrenfort E, Girovsky J, Toskovic R, Lado J L, Fernández-Rossier J and Otte A F 2016 *Nat. Nanotechnol.* **11** 926
[5] Nilius N, Wallis T M and Ho W 2002 *Science* **297** 1853
[6] Hirjibehedin C F, Lutz C P and Heinrich A J 2006 *Science* **312** 1021
[7] Nadj-Perge S, Drozdov I K, Li J, Chen H, Jeon S, Seo J, MacDonald A H, Bernevig B A and Yazdani A 2014 *Science* **346** 602
[8] Feldman B E, Randeria M T, Li J, Jeon S J, Xie Y L, Wang Z J, Drozdov I K, Bernevig B A and Yazdani A 2017 *Nat. Phys.* **13** 286
[9] Jeon S, Xie Y L, Li J, Wang Z J, Bernevig B A and Yazdani A 2017 *Science* **358** 772
[10] Kim H, Palacio-Morales A, Posske T, Rozsa L, Palotás K, Szunyogh L, Thorwart M and Wiesendanger R 2018 *Sci. Adv.* **4** eaar5251
[11] Crommie M F, Lutz C P and Eigler D M 1993 *Science* **262** 218
[12] Manoharan H C, Lutz C P and Eigler D M 2000 *Nature* **403** 512
[13] Li Q L, Cao R X and Ding H F 2020 *Appl. Phys. Lett.* **117** 060501
[14] Gomes K K, Mar W, Ko W, Guinea F and Manoharan H C 2012 *Nature* **483** 306
[15] Collins L C, Witte T G, Silverman R, Green D B and Gomes K K 2017 *Nat. Commun.* **8** 15961
[16] Kempkes S N, Slot M R, Freeney S E, Zevenhuizen S J M, Vanmaekelbergh D, Swart I and Smith C M 2019 *Nat. Phys.* **15** 127
[17] Lieb E H 1989 *Phys. Rev. Lett.* **62** 1201
[18] Tasaki H 1992 *Phys. Rev. Lett.* **69** 1608
[19] Mielke A and Tasak H 1993 *Commun. Math. Phys.* **158** 341
[20] Tasaki H 1994 *Phys. Rev. Lett.* **73** 1158
[21] Miyahara S, Kusuta S and Furukawa N 2007 *Physica C* **460–462** 1145
[22] Kopnin N B, Heikkilä T T and Volovik G E 2011 *Phys. Rev. B* **83** 220503(R)
[23] Julku A, Peotta S, Vanhala T I, Kim D H and Türmä P 2016 *Phys. Rev. Lett.* **117** 045303
[24] Weeks C and Franz M 2010 *Phys. Rev. B* **82** 085310
[25] Goldman N, Urban D F and Bercioux D 2011 *Phys. Rev. A* **83** 063601
[26] Tang E, Mei J W and Wen X G 2011 *Phys. Rev. Lett.* **106** 236802
[27] Mukherjee S, Spracklen A, Choudhury D, Goldman N, Öhberg P, Andersson E and Thomson R R 2015 *Phys. Rev. Lett.* **114** 245504
[28] Taie S, Ozawa H, Ichinose T, Nishio T, Nakajima S and Takahashi Y 2015 *Sci. Adv.* **1** e1500854
[29] Vicencio R A, Cantillano C, Morales-Inostroza L, Real B, Mejiá-Cortés C, Weimann S, Szameit A and Molina M I 2015 *Phys. Rev. Lett.* **114** 245503
[30] Diebel F, Leykam D, Kroesen S, Denz C and Desyatnikov A S 2016 *Phys. Rev. Lett.* **116** 183902
[31] Slot M R, Gardenier T S, Jacobse P H, van Miert G C P, Kempkes S N, Zevenhuizen S J M, Smith C M, Vanmaekelbergh D and Swart I 2017 *Nat. Phys.* **13** 672
[32] Drost R, Ojanen T, Harju A and Liljeroth P 2017 *Nat. Phys.* **13** 668
[33] Yan L H and Liljeroth P 2019 *Adv. Phys. X* **4** 1651672
[34] Slot M R, Kempkes S N, Knol E J, van Weerdenburg W M J, van den Broeke J J, Wegner D, Vanmaekelbergh D, Khajetoorians A A, Smith C M and Swart I 2019 *Phys. Rev. X* **9** 011009
[35] Eigler D M and Schweizer E K 1990 *Nature* **344** 524
[36] Kittel C 2005 *Fermi Surfaces and Metals* in *Introduction to Solid State Physics* (New York: Wiley) p 233
[37] Kliewer J, Berndt R and Crampin S 2000 *Phys. Rev. Lett.* **85** 4936
[38] Fiete G A and Heller E J 2003 *Rev. Mod. Phys.* **75** 933
[39] Li J T, Schneider W D and Berndt R 1997 *Phys. Rev. B* **56** 7656
[40] Mielke A 1991 *J. Phys. A* **24** 3311
[41] Shen R, Shao L B, Wang B and Xing D Y 2010 *Phys. Rev. B* **81** 041410(R)
[42] Qiu W X, Li S, Gao J H, Zhou Y and Zhang F C 2016 *Phys. Rev. B* **94** 241409(R)
[43] Lazarovits B, Szunyogh L and Weinberger P 2006 *Phys. Rev. B* **73** 045430
[44] Lounis S, Mavropoulos P, Dederichs P H and Blügel S 2006 *Phys. Rev. B* **73** 195421
[45] Madhavan V, Chen W, Jamneala T, Crommie M F and Wingreen N S 2001 *Phys. Rev. B* **64** 165412
[46] Olsson F E, Persson M, Borisov A G, Gauyacq J P, Lagoute J and Fölsch S 2004 *Phys. Rev. Lett.* **93** 206803
[47] Limot L, Pehlke E, Kröger J and Berndt R 2005 *Phys. Rev. Lett.* **94** 036805
[48] Tacca M S, Jacob T and Goldberg E C 2021 *Phys. Rev. B* **103** 245419
[49] Fernández J, Roura-Bas P and Aligia A A 2021 *Phys. Rev. Lett.* **126** 046801
[50] Fölsch S, Hyldgaard P, Koch R and Ploog K H 2004 *Phys. Rev. Lett.* **92** 056803
[51] Lagoute J, Liu X and Fölsch S 2005 *Phys. Rev. Lett.* **95** 136801
[52] Huda M N, Kezilebieke S and Liljeroth P 2020 *Phys. Rev. Res.* **2** 043426

Supplementary information:

Lieb lattices formed by real atoms on Ag(111) and their lattice constant dependent electronic properties

Xiaoxia Li†, Qili Li†, Tongzhou Ji, Ruige Yan, Wenlin Fan, Bingfeng Miao, Liang Sun, Gong Chen, Weiyi Zhang, Haifeng Ding*

†These authors contribute equally to this work

*Corresponding author: hfding@nju.edu.cn

S-1. TIGHT-BINDING METHOD

The band structure of the Lieb lattice can be derived from a tight-binding model. In it, we consider the overlap among *s*-states electrons. The Hamiltonian of the system is $H = \sum_i \varepsilon_i a_i^+ a_i - t\sum_{\langle i,j\rangle}(a_i^+ a_j + H.C.) - t'\sum_{\langle\langle i,j\rangle\rangle}(a_i^+ a_j + H.C.)$ with t and t' as the nearest-neighboring (NN) and the next-nearest-neighboring (NNN) overlap energy, respectively.

We set the onsite energy to be ε_0 for both corner- and edge-sites, and the lattice constant to be *2r*. Then the matrix form of the Hamiltonian of the system is:

$$\mathbf{H} = \begin{pmatrix} \varepsilon_0 & -2t\cos(k_x r) & -2t\cos(k_y r) \\ -2t\cos(k_x r) & \varepsilon_0 & -4t'\cos(k_x r)\cos(k_y r) \\ -2t\cos(k_y r) & -4t'\cos(k_x r)\cos(k_y r) & \varepsilon_0 \end{pmatrix}. \quad (1)$$

The energy eigenvalues are obtained by solving the secular equation:

$$\det\left|\mathbf{H} - \varepsilon\mathbf{I}_{3\times 3}\right| = \begin{vmatrix} \varepsilon_0 - \varepsilon & -2t\cos(k_x r) & -2t\cos(k_y r) \\ -2t\cos(k_x r) & \varepsilon_0 - \varepsilon & -4t'\cos(k_x r)\cos(k_y r) \\ -2t\cos(k_y r) & -4t'\cos(k_x r)\cos(k_y r) & \varepsilon_0 - \varepsilon \end{vmatrix} = 0. \quad (2)$$

For the case of $t' = 0$, the Hamiltonian can be simplified as:

$$\mathbf{H} = \begin{pmatrix} \varepsilon_0 & -2t\cos(k_x r) & -2t\cos(k_y r) \\ -2t\cos(k_x r) & \varepsilon_0 & 0 \\ -2t\cos(k_y r) & 0 & \varepsilon_0 \end{pmatrix}. \quad (3)$$

The eigenvalues can be obtained as:

$$\begin{cases} \varepsilon_1 = \varepsilon_0 \\ \varepsilon_2 = \varepsilon_0 - 2t\sqrt{(\cos^2(k_x r) + \cos^2(k_y r))} \\ \varepsilon_3 = \varepsilon_0 + 2t\sqrt{(\cos^2(k_x r) + \cos^2(k_y r))} \end{cases}. \quad (4)$$

ε_1 is a flat band. ε_2 and ε_3 are two dispersive bands. Then we employ the numerical integral method to obtain local density of states (LDOS) spectra. The corresponding LDOS spectra at the edge- and corner-sites demonstrate that there are two peaks at $E_l = \varepsilon_0 - 2t$ and $E_h = \varepsilon_0 + 2t$ at corner site, and one additional peak appears at $E_m = \varepsilon_0$ due to the flat band. Therefore, the NN overlap energy can be obtained as:

$$t = \frac{E_h - E_m}{2} \text{ or } \frac{E_m - E_l}{2}. \quad (5)$$

When $t' \neq 0$, the flat band bends near the Brillouin zone center, while it remains flat from M to Γ. Thus, it can still result a peak in the LDOS of edge-site with a small shift from ε_0 (Fig. S1(a)). The corresponding LDOS maps are shown in Fig. S1(b). Note that considering the lifetime effect of surface state electrons, we added a broadening of 0.2t in the LDOS calculation.

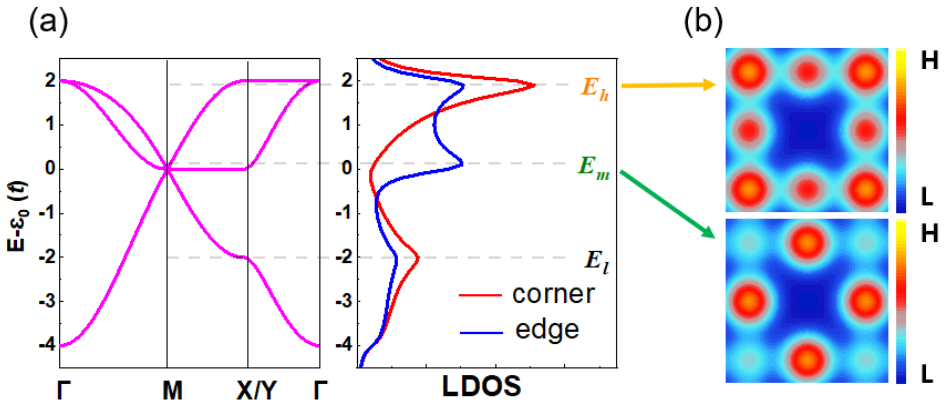

Fig. S1: (a) Calculated electronic band structure and LDOS of a Lieb lattice with t = 100 meV and $t' = 0.5t$ via tight-binding method. (b) Corresponding LDOS maps at E_h (upper) and E_m (lower).

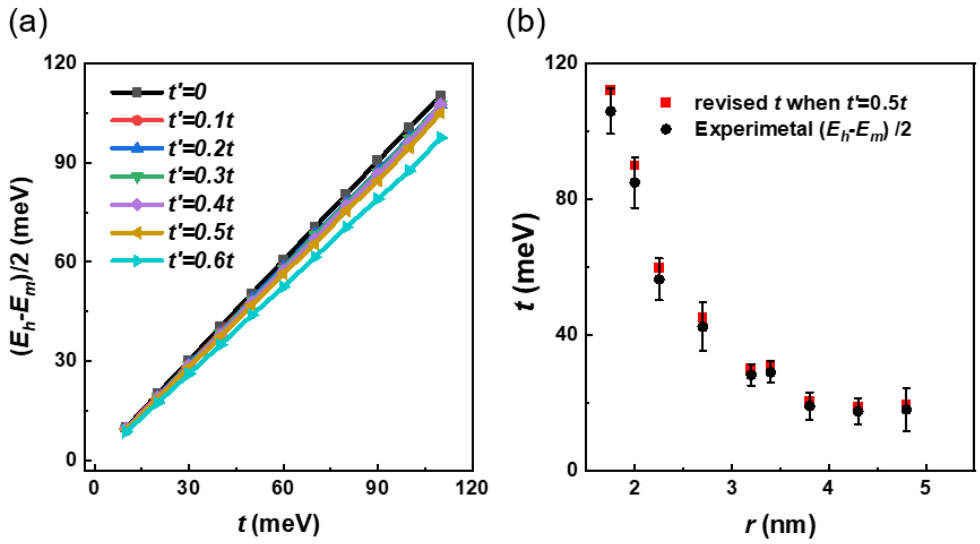

Fig. S2: (a) The calculated influence of t' on the estimation of t with the proposed method. (b) Comparison of the revised t and the experimentally obtained ones.

To evaluate the influence of t', we calculate $\frac{E_h - E_m}{2}$ as a function of t for different t' from 0 to 0.6t. As shown in Fig. S2(a), the overlap energy is exactly $\frac{E_h - E_m}{2}$ for $t' = 0$. As for $t' \neq 0$, the value of $\frac{E_h - E_m}{2}$ has a small deviation from t. It is, however, still within the experimental error bar, as shown in Fig. S2(b). Thus, we can approximately obtain:

$$t \approx \frac{E_h - E_m}{2}. \tag{6}$$

In addition, the tight-binding calculation is based on the assumption that the wavefunction of the neighboring atoms, φ_i and φ_j are orthogonal. Namely, $s_{ij} = \langle \varphi_i | \varphi_j \rangle = 0$. In ref. [18], the authors, however, obtained s = 0.15 for artificially atoms built by quantum well states with a separation of ~1.28 nm. In our experiment, the minimum separation is about 1.75 nm. It can be anticipated that s should be smaller than 0.15 in our case due to its decay property with increasing

separation. Thus, we performed the calculations for *s* from 0 to 0.15. As shown in the figure below, it has little influence on the positions of the peaks. Therefore, it has no influence on our main conclusion.

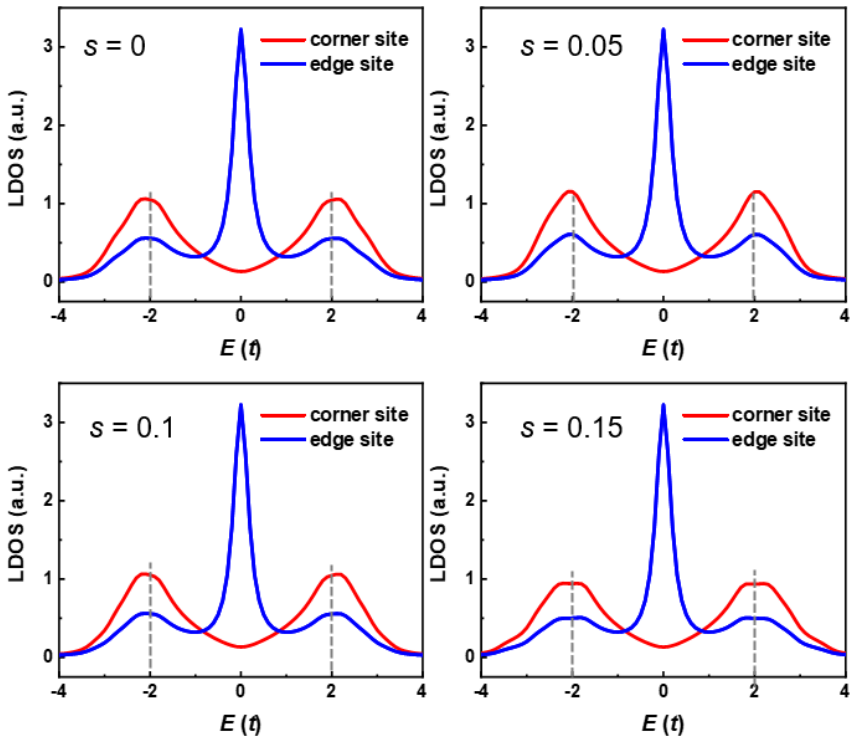

Fig. S3: The influence of *s* on the positions of characteristic LDOS peaks of a Lieb lattice.

S-2. GREEN'S FUNCTION METHOD

We consider a 4×4 Lieb lattice on the Ag(111) surface. According to the T-matrix method [1-4], the Green's function is

$$G(r,r';E) = G_0(r,r';E) + \sum_{i,j=1}^{N} G_0(r,r_i;E)T(r_i,r_j;E)G_0(r_j,r';E), \quad (7)$$

where $G_0(r,r';E) = -i\pi\rho_s H_0^{(1)}(k|r-r'|)$ is the free two-dimensional Green's function. $H_0^{(1)}(x)$ gives the zeroth-order Hankel function of the first kind and ρ_s is the density of state of the surface state. $T(r_i,r_j;E)$ is the T-matrix determined by Dyson's equation, which contains the information about the propagation between the impurities *i* and *j*:

$$T(r_i,r_j;E) = V_i\delta_{i,j} + V_i\sum_{l=1}^{N} G_0(r_i,r_l;E)T(r_l,r_j;E). \tag{8}$$

V is the scattering potential of the adatom to the surface state.

In matrix form, $\mathbf{T = V + VG_0T}$, thus we obtain $\mathbf{T = V(I - VG_0)^{-1}}$ [5], where

$$\mathbf{V} = \begin{pmatrix} \mathbf{V_1} & 0 & \cdots & 0 \\ 0 & \mathbf{V_2} & \cdots & 0 \\ \vdots & \vdots & \ddots & \vdots \\ 0 & 0 & \cdots & \mathbf{V_N} \end{pmatrix}, \tag{9}$$

and

$$\mathbf{G}_0 = \begin{pmatrix} G_0(r_1,r_1;E) & G_0(r_1,r_2;E) & \cdots & G_0(r_1,r_N;E) \\ G_0(r_2,r_1;E) & G_0(r_2,r_2;E) & \cdots & G_0(r_2,r_N;E) \\ \vdots & \vdots & \ddots & \vdots \\ G_0(r_N,r_1;E) & G_0(r_N,r_2;E) & \cdots & G_0(r_N,r_N;E) \end{pmatrix}. \tag{10}$$

For the position not on the Fe adatoms $r \neq r_i$, the LDOS is given by:

$$\rho(r;E) = -\frac{1}{\pi}\mathrm{Im}(Tr[\mathbf{G}(r,r;E)]). \tag{11}$$

For the LDOS above the corner and edge sites $r = r_i$, we treat them by taking into account the inversion effect [6]. We first calculate the LDOS of the site of concern by assuming the adatom is missing at that site, namely the LDOS of the empty site $\rho(r;E)$. Secondly, we consider the inversion effect caused by the added adatom on this site. Then, the density of state at this adatom can be obtained by the inversion relationship [7, 8]:

$$\rho_a(r;E) = -\frac{1}{\pi}\,\mathrm{Im}\,G_a(E), \tag{12}$$

where Green's function $G_a(E) = \dfrac{1}{E - E_a - \Sigma(E)}$. In it, E_a is the adsorbate energy level of a single adatom and $\Sigma(E) = \Lambda(E) - i\Delta(E)$ is the self-energy where $\Lambda(E) = \dfrac{\Delta_s \ln[(E-E_0)^2 + (\frac{\Gamma}{2})^2]}{2\pi} + const.$ and $\Delta(E) = \Delta_s \rho(r;E)\rho_s(E) + \Delta_b$. Δ_s and Δ_b are the hybridization energy of the adsorbate level with the surface and bulk states, respectively. For the Fe adatom on Ag(111), we adopt the material parameters that were used in Ref. [6], namely, $E_a = 0.21$ eV, $\Delta_s = 0.37$ eV, and $\Delta_b = 0.535$ eV. $\rho_s(E) = \dfrac{1}{2} + \dfrac{\tan^{-1}(\frac{2(E-E_0)}{\Gamma})}{\pi}$ is the surface state of the Ag(111) surface state without any adatom. $\Gamma = 38$ meV is the inverse life time of the surface state [6], and $E_0 = -65$ meV is the surface state onset energy of Ag(111) [9]. Notably, the values for all the parameters mentioned above are imported from References [6, 9]. Thus, there are no tunable parameters in our calculations.

S-3. SPECTRA COMPARISON OF THE CALCULATED AND EXPERIMENTAL RESULTS

For an isolated Fe adatom on the surface, the STM image and *dI/dV* spectrum is shown in Figs. S4(a) and S4(b). The *dI/dV* on top of the Fe adatom shows a resonance around −130 meV. Similar features were observed for Co on Au(111) [10], Cu on Cu(111) [11], and Ag and Co on Ag(111) [8]. These are localized states on top of the transition metal adatoms and are attributed to the strong coupling of the *s* state of the adatoms with the bulk and surface states of the (111) oriented noble metal substrate [12-15]. The calculated LDOS at the Fe adatom is shown in Fig.

S4(c), which shows a close similarity with the experimentally obtained *dI/dV* curve (Fig. S4(b)). The overall bending up of the *dI/dV* curves as compared to the LDOS is due to the bias dependent tunneling matrices [16]. For reference, we also show a typical *dI/dV* curve obtained on a flat Ag(111) terrace, which exhibits a onset energy at –65 meV.

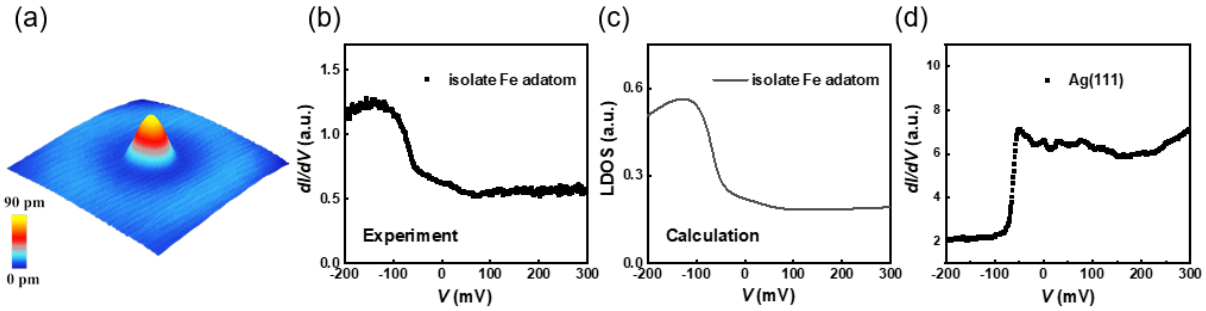

Fig. S4: (a) Morphology of an isolated Fe adatom on a wide Ag(111) terrace. ($V_{bias} = 0.05$ V, $I = 1.0$ nA). (b) The corresponding *dI/dV* spectrum. (c) The calculated LDOS of an Fe single adatom on Ag(111) by means of the Green's function method. (d) A typical experimentally obtained *dI/dV* spectrum of Ag(111) surface.

Figure S5 is the comparison between the experimental *dI/dV* curves and the numerically calculated LDOS via Green's function method. The experimentally raw data of *dI/dV* and *(dI/dV)/(I/V)* obtained with different interatomic distance *r* is shown in Figs. S5(a) and S5(b). They exhibit pronounced peaks with the width increases with decreasing *r*. This can be understood as the surface state contains a lifetime and the scattering caused by the Fe adatoms increases with decreasing *r*. So does the lifetime as well as the peak width. As *r* increases, the peaks interval decreases while the peaks positions gradually move toward lower energy. The calculation results (Fig. S5(c)) show the same trends as the experimental results. To reduce the noise and minimize

the influence of the imperfect positions of Fe adatoms in the lattice sites, we obtained *dI/dV* and *I/V* spectra at different positions of the same type of lattice sites near the middle area of the 4×4 matrix. For each lattice site, the *dI/dV* curves are averaged with more than 20 spectra, and we fitted the average curves with Gaussian function and found the peak positions. The obtained *t* with both $(E_h - E_m)/2$ and $(E_m - E_l)/2$ are shown in Fig. 2(b).

We also quantitatively analyzed the variations of the calculated peaks E_m (green arrow in Fig. S5(c)) and E_h (orange arrow in Fig. S5(c)) with *r*. Table S1 shows the comparison of the fitting parameters in $E = E_0 + C/r^2$ for the peak position E_m and E_h in the calculations and experiments. The calculation results are in good agreement with the experimental results.

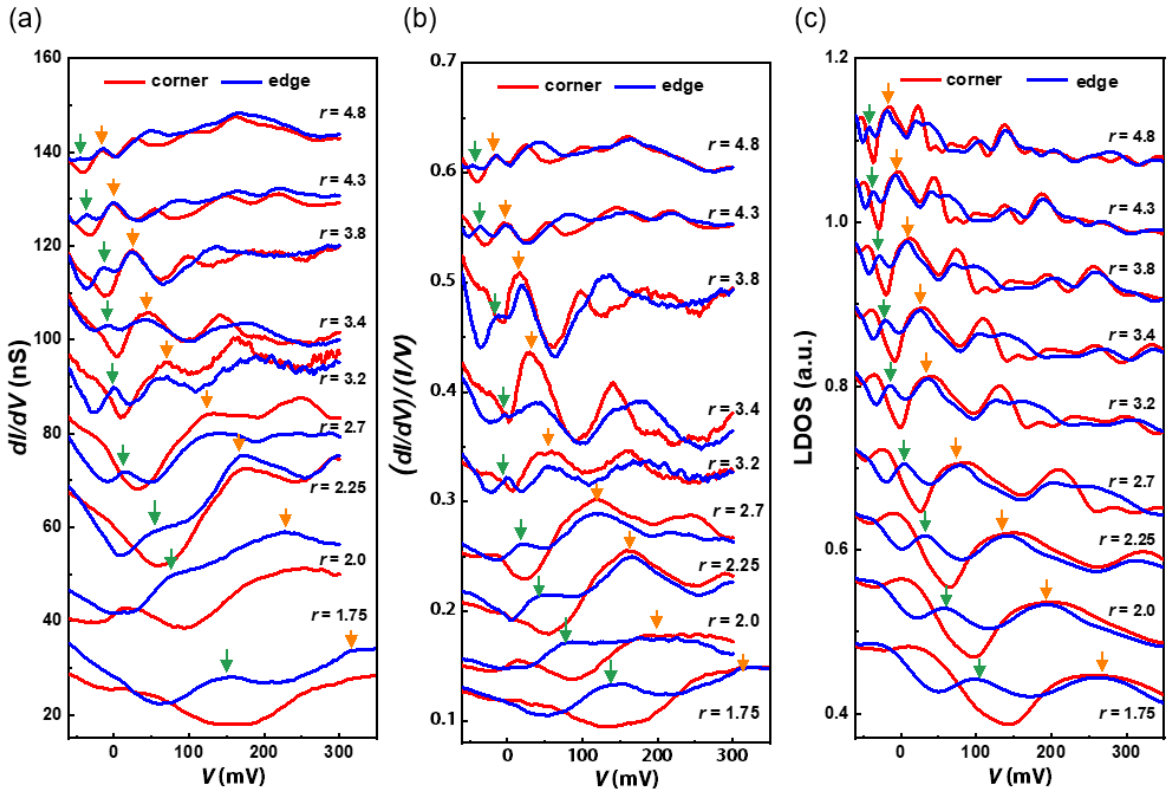

Fig. S5: (a) Raw data of *dI/dV* curves obtained at corner and edge sites with different *r*. (b) *(dI/dV)/(I/V)* spectra. (c) Calculated LDOS at the edge- and corner-sites based on the Green's

function method. The middle- and high-energy peaks positions are marked by green and orange arrows, respectively. Curves in (a), (b) and (c) are shifted for clarity.

Table S1. Fitting parameters in $E = E_0 + C/r^2$ and $\Delta E = E_\Delta + C_\Delta / r^2$ for experiments and calculations.

	E_0 or ΔE (meV)	C or C_Δ (meV•nm^2)
E_l (Exp.)	-58.8 ± 3.3	25.2 ± 19.9
E_m (Exp.)	-62.1 ± 5.2	571.0 ± 34.5
E_m (Calc.)	-64.3 ± 1.2	-505.0 ± 3.4
E_h (Exp.)	-66.5 ± 2.3	1245.5 ± 21.2
E_h (Calc.)	-61.4 ± 1.0	-1010.0 ± 9.2
$(E_h - E_m)/2$ $(E_m - E_l)/2$ (Exp.)	1.0 ± 2.2	273.9 ± 14.5
$(E_h - E_m)/2$ (Calc.)	-1.7 ± 1.2	249.3 ± 8.1

We note that for both the raw data of *dI/dV* spectra and the normalized (*dI/dV*)/(*I/V*) curves, there is a shoulder at the corner site, e.g. around 50 mV for r = 1.75 nm, which also exists in the calculated results with the Green's function method. We find it also exhibits an inverse square relationship with r. To analyze its origin, we plotted the peak energy as the function of r. After a careful analysis, we found that it is related with the eigen energy of the corral marked by the dashed circle in Fig. S6(a). The eigen energy inside of a circular corral is $E_{|n,l\rangle} = E_0 + \hbar^2 k_{n,l}^2 / (2m^*)$, where $k_{n,l} = z_{n,l} / R$ with (n,l) as the quantum number [17]. Here, $\hbar$ is the reduced Planck constant, $z_{n,l}$ is the n^{th} zero crossing of l^{th} order Bessel function and m^* is the effective mass of the surface state. $E_{n,l}$ refers to the state related to the quantum number (n,l). The energy position in the LDOS calculated with the Green's function method agrees well with the eigen energy $E_{1,1}$ of the

marked corral (Fig. S6(b)). Due to the weak strength of the confinement, it appears as a shoulder in LDOS.

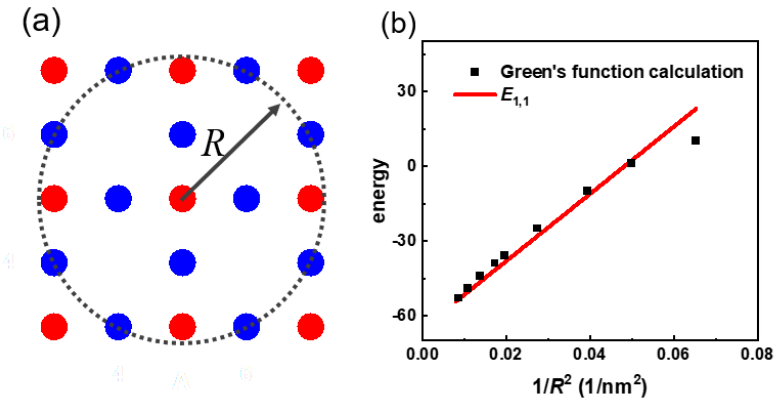

Fig. S6: (a) The outer circular corral with radius R. (b) The comparison of the eigen energy $E_{1,1}$ of the circular corral with the energy of the shoulder at the corner site calculated by Green's function.

Above, we discussed the calculated results for an ideal lattice. In real experiments, it is difficult to position the Fe adatoms to the ideal lattice sites, especially a Lieb lattice has a 4-fold symmetry while the Ag(111) substrate has a 6-fold symmetry. We find that the experimental error margin for positioning the Fe adatoms is ~0.2 nm in lateral. To accommodate the influence of the inaccuracy of Fe adatom positioning, we also made the calculation for a similar structure with the adatom randomly distributed within 0.2 nm away from the ideal lattice site. As shown in Fig. S7, the calculated spectra at both corner and edge sites are similar for the cases with and without disorder. Thus, we conclude that the effect of small disorder is negligibly small.

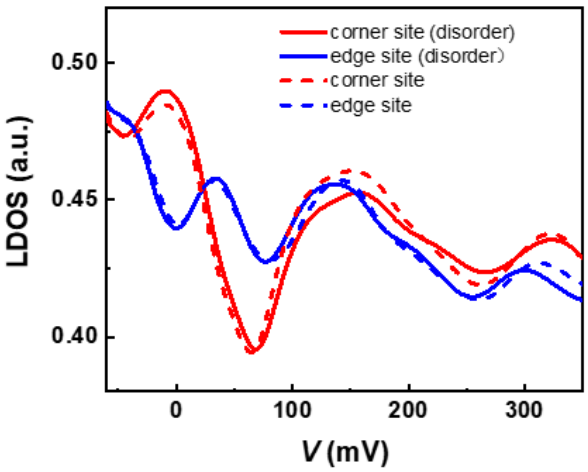

Fig. S7: Comparison of the calculated spectra with and without disorder.

S-4. THE INFLUENCE OF THE UNIT CELL SIZE

According to the Green's function method, we calculated the LDOS for a 4×4 and 5×5 Lieb lattice with $2r$ = 4.5 nm, respectively. We found that the curves are almost the same for these two different sizes (Fig. S8). Thus, we conclude that the 4×4 lattice is sufficient to demonstrate the properties of Lieb lattice. This is in good agreement with previous analysis [18, 19].

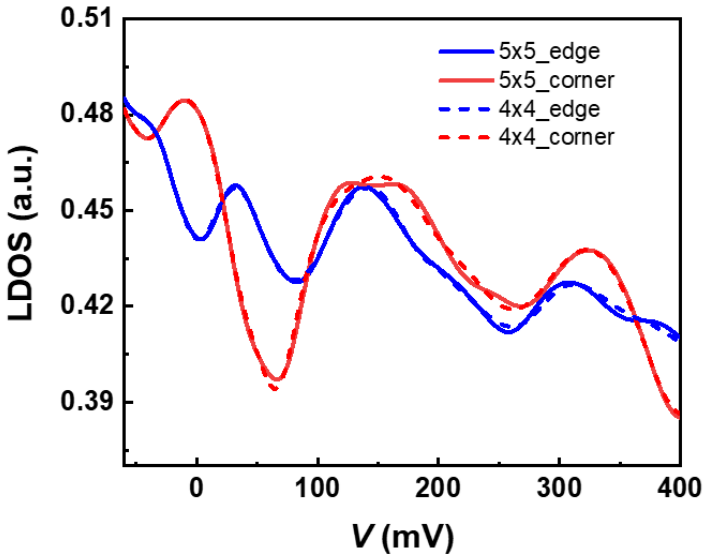

Fig. S8: The calculated LDOS for a 4×4 and 5×5 Lieb lattice via the Green's function method. The lattice constant $2r$ is 4.5 nm.

S-5. LDOS MAPS COMPARISON OF THE CALCULATED AND EXPERIMENTAL RESULTS

To focus our discussion on the distance dependent overlap energy, the LDOS maps in Fig. 3(b) is obtained through the tight-binding calculations only. The scattering of the surface state is neglected. The features at the middle of the Lieb lattice at energy E_m and the ring-shaped features at E_h in Fig. 1(c) are the interference pattern caused by the scattering of the surface state. To further confirm this, we calculated the LDOS map utilizing the Green's function method. As shown in Fig. S9, though not exactly the same, the calculations including the scattering effect do represent close similarity with the experimental observations and the features mentioned above are essentially shown. We note that, in our Green's functions calculation, we only consider the scattering of the surface state by the Fe adatom as well as the hybridization of Fe 4*s* state and the surface state of Ag(111). For more accurate analysis, first-principle calculations may be needed.

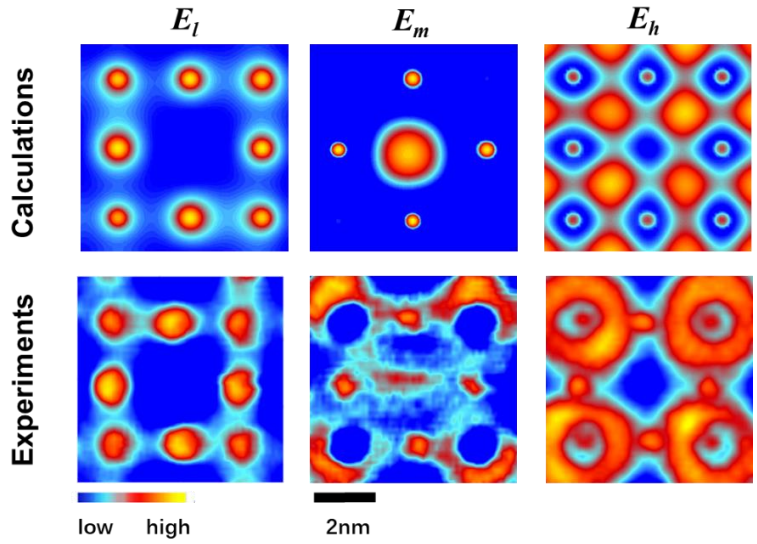

Fig. S9: Comparison of the calculated LDOS maps obtained with Green's function method and the experimental results at E_l, E_m and E_h (r = 2.25 nm).

S-6. ARTIFICIAL IRON LIEB LATTICE ON SILVER(100)

We constructed a series of Lieb lattices on Ag(100) in a similar way as we did on Ag(111). The representative topographic image is shown in the inset of (Fig. S10(a)). The *dI/dV* spectra of corner site, edge site and an isolated adatom are almost the same even when we approached a value of *r* of only 1 nm. Namely, no apparent electronic signal of Lieb lattice is observed. Because it is difficult to construct a Lieb lattice with smaller lattice constant, we constructed twin atoms on Ag(100) and investigated the *dI/dV* on top of them with different interatomic separations as shown in (Fig. S10(b)). It is found that there are no apparent differences in *dI/dV* between the spectra obtained on top of the twin atoms with *r* approaching 0.64 nm and that obtained on an isolated adatom (r > 2.8 nm).

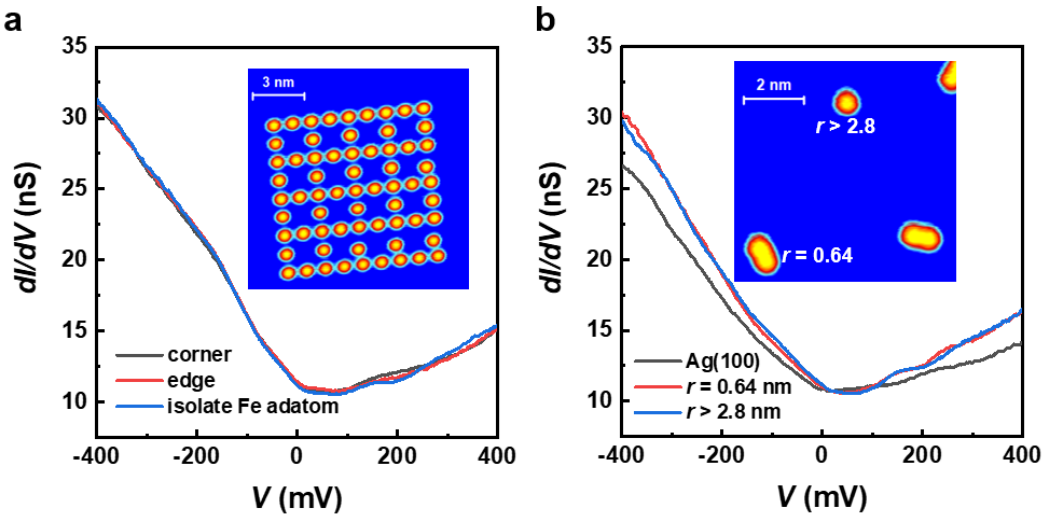

Fig. S10: (a) STM morphologic image and corresponding *dI/dV* spectra at corner- and edge-sites of a 4×4 Lieb lattice constructed by Fe adatoms on Ag(100) with r = 1.25 nm. The spectrum of a single isolated Fe adatom is also included for comparison. (b) STM image and *dI/dV* spectra of Fe adatoms on Ag(100) (STM image: $V_{bias} = 0.5$ V, $I = 1.0$ nA. *dI/dV* spectra: $V_{bias} = 0.1$ V, $I = 1.0$ nA, $V_{mod} = 20$ mV).

Reference

[1] Fiete G A and Heller E J 2003 *Rev. Mod. Phys.* **75** 933-948.
[2] Biswas R R and Balatsky A V 2010 *Phy. Rev. B* **81** 233405.
[3] Fu Z-G, Zhang P, Wang Z and Li S-S 2011 *Phy. Rev. B* **84** 235438.
[4] She J H, Fransson J, Bishop A R and Balatsky A V 2013 *Phy. Rev. Lett.* **110** 026802.
[5] Zheng C, Li Q L, Miao B F, Sun L, Wang R, Li X X and Ding H F 2017 *Phy. Rev. B* **96** 235444.
[6] Li Q L, Li X X, Miao B F, Sun L, Chen G, Han P and Ding H F 2020 *Nat. Commun.* **11** 1400.
[7] Kliewer J, Berndt R and Crampin S 2000 *Phys. Rev. Lett.* **85** 4936-4939.
[8] Limot L, Pehlke E, Kröger J and Berndt R 2005 *Phys. Rev. Lett.* **94** 036805.
[9] Li J T, Schneider W D and Berndt R 1997 *Phys. Rev. B* **56** 7656-7659.
[10] Madhavan V, Chen W, Jamneala T, Crommie M F and Wingreen N S 2001 *Phys. Rev. B* **64** 165412.
[11] Olsson F E, Persson M, Borisov A G, Gauyacq J P, Lagoute J and Fölsch S 2004 *Phys. Rev. Lett.* **93** 206803.
[12] Lazarovits B, Szunyogh L and Weinberger P 2006 *Phys. Rev. B* **73** 045430.
[13] Lounis S, Mavropoulos P, Dederichs P H and Blügel S 2006 *Phys. Rev. B* **73** 195421.

[14] Fernández J, Roura-Bas P and Aligia A A 2021 *Phys. Rev. Lett.* **126** 046801.
[15] Tacca M S, Jacob T and Goldberg E C 2021 *Phys. Rev. B* **103** 245419.
[16] Bonell D 2001 *Scanning Probe Microscopy and Spectroscopy* (Wiley).
[17] Crommie M F, Lutz C P and Eigler D M 1993 *Science* **262** 218-220.
[18] Drost R, Ojanen T, Harju A and Liljeroth P 2017 *Nat. Phys.* **13** 668-672.
[19] Slot M R, Gardenier T S, Jacobse P H, van Miert G C P, Kempkes S N, Zevenhuizen S J M, Smith C M, Vanmaekelbergh D and Swart I 2017 *Nat. Phys.* **13** 672-677.